Cell Reports

Resource

Multi-label *in vivo* STED microscopy by parallelized switching of reversibly switchable fluorescent proteins

Graphical abstract

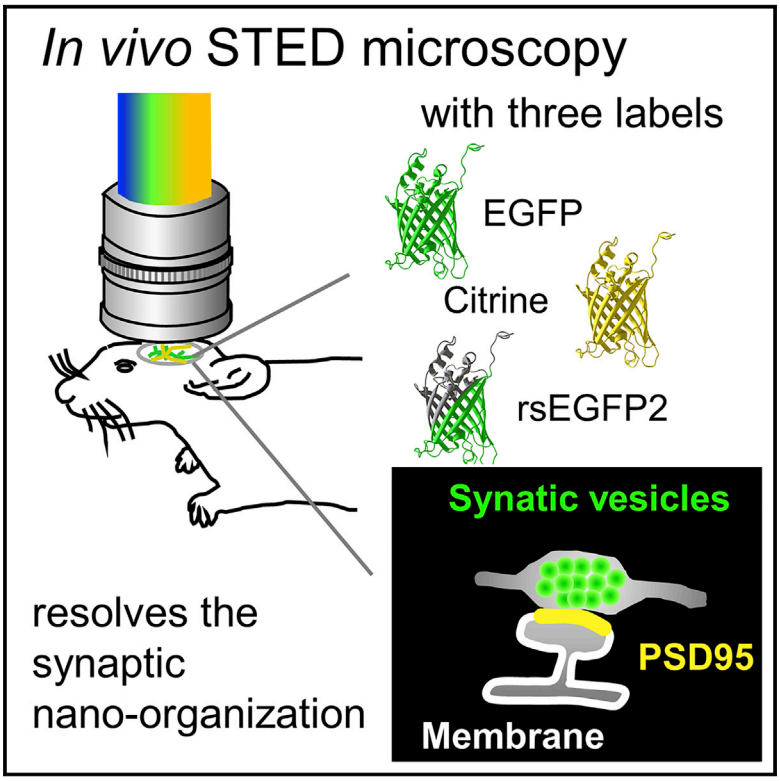

Authors

Katrin I. Willig, Waja Wegner, Antonia Müller, Valérie Clavet-Fournier, Heinz Steffens

Correspondence

kwillig@em.mpg.de

In brief

Synaptic proteins and receptors form nanostructures that cannot be resolved with conventional light microscopy. Willig et al. use *in vivo* STED microscopy to image three labels in the mouse cortex with nanoscale resolution. This technique enables, for example, quasi-simultaneous *in vivo* super-resolution imaging of pre- and postsynaptic nanostructures.

Highlights

- *In vivo* super-resolution STED microscopy of three labels in cortex of mice
- Nanoscale imaging of pre- and postsynapse *in vivo*
- Temporal sequential imaging of reversibly switchable fluorescent proteins (RSFPs)
- Parallelized switching schema enables quasi-simultaneous imaging

Willig et al., 2021, Cell Reports *35*, 109192
June 1, 2021
https://doi.org/10.1016/j.celrep.2021.109192

CellPress

Cell Reports

CellPress
OPEN ACCESS

Resource

Multi-label *in vivo* STED microscopy by parallelized switching of reversibly switchable fluorescent proteins

Katrin I. Willig,[1,2,3,6,*] Waja Wegner,[1,2] Antonia Müller,[1,2,4] Valérie Clavet-Fournier,[1,2,5] and Heinz Steffens[1,2]

[1]Optical Nanoscopy in Neuroscience, Center for Nanoscale Microscopy and Molecular Physiology of the Brain, University Medical Center Göttingen, Göttingen, Germany

[2]Max Planck Institute of Experimental Medicine, Göttingen, Germany

[3]Cluster of Excellence "Multiscale Bioimaging: From Molecular Machines to Networks of Excitable Cells" (MBExC), University of Göttingen, Göttingen, Germany

[4]Collaborative Research Center 889, University of Göttingen, Göttingen, Germany

[5]Göttingen Graduate Center for Neurosciences, Biophysics, und Molecular Biosciences (GGNB), Göttingen, Germany

[6]Lead contact

*Correspondence: kwillig@em.mpg.de

https://doi.org/10.1016/j.celrep.2021.109192

SUMMARY

Despite the tremendous success of super-resolution microscopy, multi-color *in vivo* applications are still rare. Here we present live-cell multi-label STED microscopy *in vivo* and *in vitro* by combining spectrally separated excitation and detection with temporal sequential imaging of reversibly switchable fluorescent proteins (RSFPs). Triple-label STED microscopy resolves pre- and postsynaptic nano-organizations *in vivo* in mouse visual cortex employing EGFP, Citrine, and the RSFP rsEGP2. Combining the positive and negative switching RSFPs Padron and Dronpa-M159T enables dual-label STED microscopy. All labels are recorded quasi-simultaneously by parallelized on- and off-switching of the RSFPs within the fast-scanning axis. Depletion is performed by a single STED beam so that all channels automatically co-align. Such an addition of a second or third marker merely requires a switching laser, minimizing setup complexity. Our technique enhances *in vivo* STED microscopy, making it a powerful tool for studying multiple synaptic nano-organizations or the tripartite synapse *in vivo*.

INTRODUCTION

Super-resolution techniques have become an indispensable tool in cell biology. These novel light microscopy techniques, however, are still rarely applied for *in vivo* or intravital imaging. Especially for brain research, *in vivo* measurements are inevitable because the whole neuronal network is only fully functional in the whole organism. This is especially essential for the study of learning and memory. Growing evidence suggested recently that nanoscale protein structures in the brain might influence synaptic transmission. For example, current studies propose that synaptic proteins and receptors are organized in a nano-architecture that is not visible with conventional microscopy and thus requires super-resolution (Chen et al., 2018; Herring and Nicoll, 2016). Moreover, recent *in vitro* studies suggest that pre- and postsynaptic structures are aligned and form nano-columns whose observation requires simultaneous super-resolution of three labels to resolve the synapse and receptors. In addition, investigating the nanophysiology of the tripartite synapse *in vivo*, which is formed between the pre- and postsynapse and small protrusions of astrocytes, calls for super-resolution *in vivo* imaging of three labels. Of all super-resolution techniques, stimulated emission depletion (STED) microscopy stands out for its potential to image in the living animal. However, imaging multiple labels simultaneously in the living animal has remained highly challenging ever since the first realization of *in vivo* STED microscopy in 2012 (Berning et al., 2012).

Nevertheless, imaging multi-labels simultaneously to address structural and/or functional correlations is essential throughout biological studies, and thus many efforts have been made to push for multi-color super-resolution microscopy. The specific challenge of multi-color STED microscopy is that STED microscopy requires depletion with light of a wavelength in the emission spectrum of the fluorescent dye and, thus, both excitation and depletion light. Performing STED multi-color imaging simply by adding spectrally separate fluorescent labels as in conventional fluorescence microscopy, however, would render STED microscopy highly complex and expensive by integrating multiple laser lines. In addition, the high power of the STED beam would excite and thus photobleach red-shifted dyes (Blom and Widengren, 2017). Therefore, most current multi-color approaches rely on a single depletion beam that renders all images automatically co-aligned but requires the wavelength of each fluorescence emission to be close to the STED beam's

(Blom and Widengren, 2017). This can be achieved either by combining a long Stokes shift dye with a conventional dye and/or by combining two closely emitting dyes (Göttfert et al., 2013; Sidenstein et al., 2016). By hyperspectral detection, this approach can be extended to multiple dyes (Winter et al., 2017). Alternative approaches utilize separation by fluorescence lifetime (Bückers et al., 2011) or transient binding (Beater et al., 2015). For not all of these approaches, however, a live-cell compatible labeling strategy exists. Thus, multi-label STED imaging appears prohibitively complex and restricts *in vivo* multi-labeling strategies.

The most common live-cell and *in vivo* labeling technique is the expression of fusion proteins with fluorescent proteins such as GFP. Such labels, however, in general show neither large variations in lifetime nor a large Stokes shift. Therefore, two-color STED imaging of living cells utilizes mainly fluorescent molecules that are spectrally close, such as EGFP and EYFP (Tønnesen et al., 2011), or two organic molecules, such as, for instance, silicon-rhodamine (SiR) and ATTO590 (Bottanelli et al., 2016). Organic dyes often provide brighter and more photo-stable labels than fluorescent proteins (Schneider and Hackenberger, 2017), and genetic labeling can be performed, for instance, via Halo and SNAP tags (Bottanelli et al., 2016). However, the separate labeling step renders *in vivo* applications complex (Masch et al., 2018) and is probably incompatible in principle with chronic imaging. But most importantly, none of these approaches are extendable to the imaging of three labels, which is essential, for instance, to resolve the pre- and postsynaptic structures together with functional correlates such as receptors.

Here, we introduce an approach to perform *in vivo* STED microscopy of three different labels quasi-simultaneously using only fluorescent proteins. To this end, we build on two-color STED microscopy of EGFP and EYFP (or Citrine) and augment it by a reversibly switchable fluorescent protein (RSFP). Choosing a RSFP in the same spectral range as EGFP and EYFP enables recording of images sequentially in time. RSFPs are key to RESOLFT (reversible saturable optical fluorescence transition) microscopy, a coordinate-targeted super-resolution technique that uses the *cis-trans* isomerization of RSFPs to switch off fluorescence and achieve super-resolution (Eggeling et al., 2015). RSFPs can be switched from a fluorescent on state to a fluorescent off state reversibly by light of different wavelength (Jensen et al., 2020). Faster than RESOLFT microscopy, we here use STED to read out a super-resolution image when the RSFP is in the on state. Thus, we record super-resolution STED images of EGFP, EYFP, or Citrine and alternately of a RSFP. By this method, three labels can be super-resolved using a two-color STED microscope augmented by two simple lasers for switching the RSFP. Excitation, stimulated depletion, and detection of the RSFP are then possible with the same excitation and detection channels as used for EGFP and EYFP/Citrine. By switching the RSFP on and off between lines, all three labels are recorded quasi-simultaneously line by line. Switching back and forth may in principle substantially decelerate image acquisition, because the time for switching of RSFPs is at least 10-fold slower than STED image recording. To avoiding slowdown and achieve fast switching, we introduce a parallelized switching approach based on line-pattern illumination. Employing similar principles, we further demonstrate quasi-simultaneous imaging of two RSFPs with a simple one-color STED microscope. RSFPs can exhibit antagonistic switching behavior of either negative switching whereby the light eliciting fluorescence induces the off-switching or positive switching such that the on-switching is induced while reading out the fluorescence. By combining the positive switching Padron and negative switching Dronpa-M159T, simple switching lasers are sufficient to record dual-label STED images with a single excitation laser and detection channel (Willig et al., 2011). However, with this approach, the positive and negative RSFPs had to be recorded sequentially in separate images (Willig et al., 2011). The parallelized switching approach we present here now enables quasi-simultaneous imaging.

Thus, we present here a proof of principle of triple-label *in vivo* STED microscopy. By advancing a two-color STED microscope with intelligent switching, our method is relatively simple, and by relying on fluorescent proteins, it is capable of imaging living cells *in vitro* and *in vivo*.

RESULTS

Triple-label STED microscopy utilizing conventional and RSFPs

For STED microscopy of three different labels, we combined spectral separation of EGFP and EYFP or Citrine with alternated switching of a green-emitting RSFP as the third label. A custom-built STED microscope (Willig et al., 2014) was modified as follows. As sketched in Figure 1A, two pulsed excitation lasers, two lasers for switching of RSFPs (Figure 1B), and the STED laser were combined and coupled into a microscope stand after passing a scanning unit and relay optics. To spectrally separate the green and yellow fluorescence of EGFP and EYFP/Citrine, we incorporated a pulsed excitation at 483 nm (Exc1) to primarily excite EGFP and at 520 nm to primarily excite EYFP/Citrine (Exc2) (Figure 1C). The spectral separation is complemented by a selective detection of EGFP and EYFP/Citrine via two detection channels, Det1 and Det2 (Figure 1D). For the third label, we utilize, for example, the RSFP rsEGFP2 (Figure 1B) (Grotjohann et al., 2012), which is spectrally overlapping with EGFP and Citrine (Figures 1C and 1D) but can be selectively switched on by UV light and off by blue light. Therefore, we incorporated two continuous wave lasers for switching, one at 405 nm for on-switching (Switch2) (Figure 1A) and another at 488 nm for off-switching (Switch1) (Figure 1A). All three fluorescent proteins are subject to stimulated depletion at 595 nm. To increase the switching speed of the RSFP, we parallelized the switching within one line of recording. We thus implemented cylindrical lenses into both switching beams so that a line pattern instead of a diffraction-limited focal spot is created in the focal plane for the switching beams (Figure S1). The line illumination pattern is aligned parallel to the x axis of the image, which is the fast-scanning axis. Thus, ~30 μm along the x axis is illuminated simultaneously by the switching light (Figure S1A) instead of ~200 nm when illuminating with a diffraction-limited spot (Figure S1B). To record a line of an image, each line is scanned multiple times; each line scan either performs image acquisition by scanning the diffraction-limited

CellPress
OPEN ACCESS

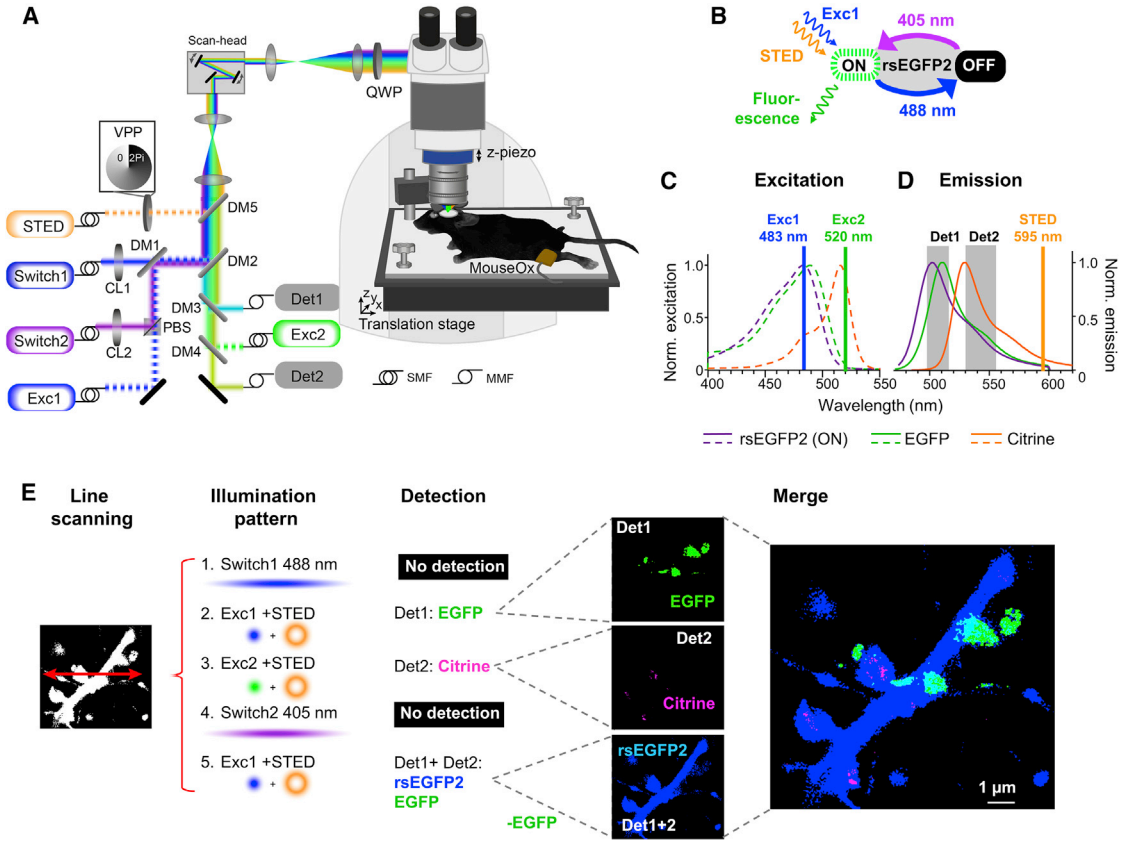

Figure 1. Custom-built STED microscope and conception for triple-label nanoscopy

(A) Two pulsed excitation beams (Exc1/2), two continuous wave laser beams incorporating a cylindrical lens (CL) for switching (Switch1/2), and a pulsed STED beam are combined via dichroic mirrors (DMs) and a polarizing beam-splitter cube (PBS); all five beams are coupled into an upright microscope after passing a scan head and relay optics.

(B) The reversibly switchable (rs) fluorescent protein rsEGFP2 is switched to the fluorescent on state by 405 nm light and to the off state by 488 nm.

(C and D) Triple labeling: EGFP is selectively excited at 483 nm and Citrine at 520 nm (C); dual detection to separately detect EGFP (Det1) and Citrine (Det2) (D); rsEGFP2 is excited at 483 nm and detected after on-switching in Det1 and Det2 (B–D).

(E) Scanning schema: each line is recorded five times with the following illumination pattern and detection channels: (1) blue switching beam to switch off rsEGFP2; (2) excitation and detection of EGFP; (3) excitation and detection of Citrine; (4) switching on rsEGFP2; and (5) excitation and detection of rsEGFP2 and EGFP. Image subtraction of EGFP to gain rsEGFP2 image. STED is optionally switched on for super-resolution.

Det, detection; MMF, multi-mode fiber; QWP, quarter wave plate; SMF, single-mode fiber.

excitation spot and detecting the fluorescence or performs parallelized switching by illumination (and scanning) with the line profile. In detail, the following illumination schemas are performed for each line per image (Figure 1E): first, the RSFP is switched off by illumination with a blue line pattern. Thereafter, EGFP is read out by scanning with a blue excitation spot and detecting its fluorescence in the first channel (Det1) followed by another scan of the same line with a green excitation spot and read out at the second detection channel (Det2) to record Citrine. Then, a line pattern of UV light (405 nm) is moved to switch on the RSFPs, leaving all conventional fluorescent proteins in an emissive on state. rsEGFP2 together with EGFP and a small fraction of Citrine cross-talk is read out with blue excitation, and the fluorescence is collected in both channels (Det1+Det2) and summed up. An image is recorded by repeating this scanning schema for each line along the y axis. The selective image of rsEGFP2 is obtained by subtracting the image that was recorded when rsEGFP2 was in the off state. To record super-resolution STED images of all three labels, the STED beam is switched on additionally in all lines recording fluorescence, but not in the switching lines. To determine the STED resolution, we labeled F-actin with each fluorescent protein separately in neuronal cultures and performed live-cell STED imaging. We obtain a resolution of ~66 nm for EYFP, ~89 nm for EGFP, and ~79 nm for rsEGFP2 (Figure S2). Thus, all fluorescent proteins performed similarly well, and the best resolution was obtained with EYFP, the most red-shifted of the three.

Acquisition and switching schemas of RSFPs to minimize cross-talk

Key to the method we present here is the switching capability of the RSFP in both switching contrast, which is the ratio of fluorescence between the on and off state, and the switching speed. We thus investigated these parameters for three different RSFPs: rsEGFP2, which expresses very well in mammalian cells, switches fast, and is

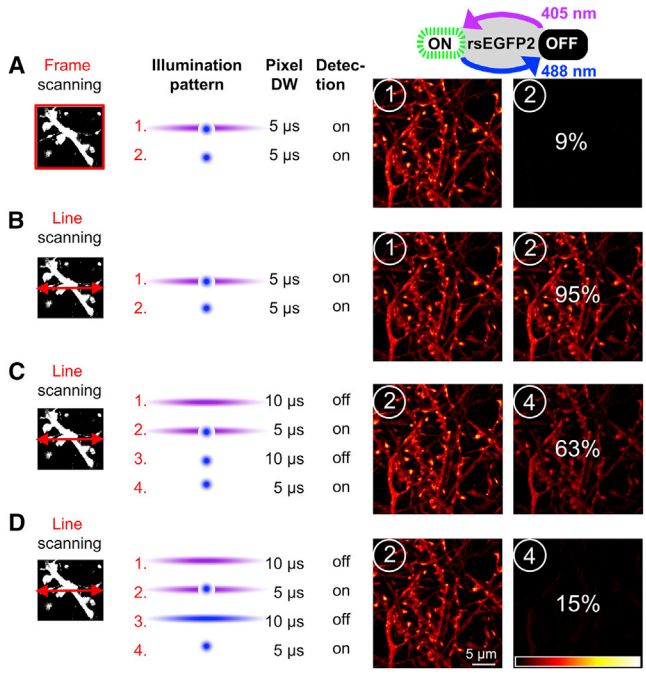

Figure 2. Comparison of switching modalities for rsEGFP2

(A–D) Switching schema tested on Lifeact-rsEGFP2 expression labeling F-actin in living neurons. (A) Frame-by-frame scanning: image-by-image recording with (1) and without (2) UV light switches off rsEGF2 to 9% of the on state. (B–D) Line-by-line scanning modalities: (B) marginal off-switching to 95% by scanning each line alternatingly with (1) and without (2) UV light. (C and D) Repeating the line scan two times for switching only (line 1 and 3) and two times for image acquisition (line 2 and 4) improves the on/off contrast to ~63%. Parallelized switching with a blue line profile (D) reduces the remaining fluorescence in the off state down to 15%. All images were recorded at the same position with the same pixel size of 30 × 30 nm and were normalized to the same maximum brightness.

See also Figure S3. DW, dwell time.

a true monomer (Grotjohann et al., 2012); Dronpa-M159T, which is as well a negative switching RSFP with superior switching speed (version 2.0) (Willig et al., 2011); and Padron, a RSFP with a positive switching mechanism (version 2.0) (Willig et al., 2011). All three RSFPs emit in the wavelength range of EGFP and Citrine, and the latter two we had previously used for STED microscopy (Willig et al., 2011). First, we tested the on-off-switching capability of these RSFPs by a sequential, frame-by-frame image recording as we have already carried out in our previous publication on dual-label STED microscopy (Willig et al., 2011). Therefore, we recorded two consecutive confocal images, one with simultaneous UV light illumination and one without. Indeed, all three RSFPs switched off with a good contrast; rsEGFP2 switched off to 9% (Figure 2A), Dronpa-M159T to 3% (Figure S3A), and Padron to 11% (Figure S3E). For live-cell imaging, however, a frame-by-frame recording of two different proteins of interest is unsuitable because intrinsic movement of the proteins most likely disturbs the spatial relation of these proteins between sequential frames rendering colocalization studies impossible. Moreover, extrinsic factors, such as drift of the scanning area or movement due to the vital function of a living animal between consecutive frames, are hampering channel overlap. Thus, we tested different scanning schemas to switch channels between sequential recordings of lines to record all channels quasi-simultaneously in an alternating fashion. First, we changed the scanning schema from frame-by-frame switching and image recording to line-by-line switching and recording while maintaining the pixel size and dwell time per pixel. We recorded each line twice, first of all by scanning with the spot of the blue excitation laser to record a confocal image and then the same line again with additional UV light for switching. Here, the switching contrast was marginal for all three proteins tested (95% remaining fluorescence in the off state for rsEGFP2, Figure 2B; 86% for Dronpa-M159T and 98% for Padron, Figures S3B and S3F). The low switching contrast shows that the illumination time was not sufficient to switch a majority of the molecules to the off state. Thus, a simple line-by-line scanning with and without UV light is not effective. We now repeated the line scan several times to enhance the switching time and decouple the switching from image recording. Thus, we scanned each line four times. The first line scan switched with the UV line pattern, the second line scan detected molecules switched on by UV light, the third line scan switched with blue light, and every fourth line scan detected molecules switched on by blue light. This scanning schema gave us the possibility to set the time for switching and image recording individually. With a 5-µs pixel dwell time for image detection and 10 µs for switching, we improved the switching contrast to 63% for rsEGFP2 (Figure 2C); similarly, switching contrast was improved to 17% for Dronpa-M159T (Figure S3C) and to 39% for Padron (Figure S3G). Please note that the positive switching Padron was detected in line 4 instead of line 2. To demonstrate the benefit of our line pattern illumination for switching, we substituted the spot switching in line 3 with blue line pattern illumination without changing any other setting. Thus, we improved the off-switching contrast to 15% for rsEGFP2 (Figure 2D), 3% for Dronpa-M159T (Figure S3D), and 20% for Padron (Figure S3H). Therefore, both rsEGFP2 and Dronpa-M159T could be switched with similar contrast as in the frame-by-frame scanning schema. Please note that all images were recorded with the same pixel dwell time of 5 µs for image recording, whereas the pixel dwell time for switching was slightly different for all three RSFPs. The switching times were optimized for switching with the UV and blue line illumination pattern (Figures 2D, S3D, and S3H) for each RSFP individually and are therefore slightly different between the different RSFPs. As expected, the dwell time for switching was shortest for the fast-switching Dronpa-M159T.

However, although we improved the switching contrast, there remains the question whether this was due to an improvement in the off-switching or on-switching. To address this question, we have performed the different switching schemas mainly at the same position, recorded all images with the same pixel dwell time, and scaled the images to the same maximum intensity. It is evident from the images that the negative switching RSFPs rsEGFP2 (Figures 2A–2D) and Dronpa-M159T (Figures S3B–S3D) showed similar on-state fluorescence in all scanning modes while putative off-state images changed brightness. In other words, our advanced switching schema with blue line illumination pattern improved the off-switching of rsEGFP2 and Dronpa-M159T. In contrast, the positive switching Padron showed the opposite behavior; pure line-by-line switching barely

switched Padron to the on state, and thus the images in Figure S3F were dark. Additional switching time with line illumination pattern increased the brightness in the on state (Figure S3H); however, the brightness was still slightly lower than in frame-by-frame scanning (Figure S3E). To conclude, the crucial and limiting parameter for switching of the tested RSFPs is the off-switching of the negative switching RSFPS and the on-switching of the positive switching RSFP, which are both performed by blue light. Taken together, switching with a line illumination pattern parallelizes the switching of RSFPs and thus minimizes the switching time. This scanning schema improves the switching contrast and image brightness to values similar to on-off switching between image frames and thus enables quasi-simultaneous imaging of different fluorescent labels.

Triple-label *in vivo* STED microscopy visualizes synaptic morphology and nano-organization

To demonstrate the potential of triple-label STED microscopy, we labeled pre- and postsynaptic elements in the visual cortex and performed *in vivo* imaging of the anesthetized mouse through a cranial window. Therefore, we generated recombinant adeno-associated viral particles (rAAVs), which are well established for *in vivo* use, encoding for fusion proteins of EGFP, Citrine, and rsEGFP2. As a presynaptic marker, we chose the synaptic vesicle protein synaptophysin, which we expressed as a fusion protein with EGFP. To label the postsynaptic spine morphology, we expressed myr-rsEGFP2-LDLR(Ct), a combination of a myristoylation site (myr), the RSFP rsEGFP2, and the C-terminal (Ct) cytoplasmic domains of low-density lipoprotein receptor (LDLR), which has been proved to be a potent marker for the dendritic membrane (Kameda et al., 2008). To visualize the postsynaptic side of glutamatergic synapses, we expressed the transcriptionally regulated antibody-like protein PSD95-FingR fused to Citrine that has been shown to label endogenous PSD95 (Gross et al., 2013). For viral transduction, we anesthetized the mouse and drilled a small hole above the visual cortex of the left hemisphere of the mouse (Figure 3A, injection side; see STAR Methods for coordinates and details). rAAVs encoding for synaptophysin-EGFP were injected at an angle of $\alpha = 30^{\circ}$ to the vertical into the dorsal lateral geniculate nucleus (dLGN), the visual thalamic structure (Figure 3B). Neurons of the dLGN send projections to layer 1, as well as deeper layers of the primary visual cortex (Cruz-Martín et al., 2014). Through the same opening, but at a larger angle $\alpha = 70^{\circ}$ to the vertical, we injected rAAV encoding the postsynaptic labels myr-rsEGFP2-LDLR(Ct) and PSD95-FingR-Citrine into layer 5 of the visual cortex (Figure 3B). The coding region for the fusion proteins of these rAAVs was floxed and therefore the expression cre dependent. We thus co-injected cre recombinase-expressing rAAVs at low concentration to adjust the density of labeled neurons. About 3 weeks after transduction, the mice were anesthetized and a cranial window was inserted over the visual cortex as previously described (Steffens et al., 2020). *In vivo* STED microscopy was performed at superficial layer 1 aiming at synapses formed between thalamocortical axonal projections and apical dendrites of layer 5 neurons (Figure 3C). Figures 3D–3G show STED images of all three labels: accumulations of synaptic vesicles in boutons are shown in green, the dendritic membrane is shown in white, and the postsynaptic density protein PSD95 is shown in magenta. All channels were recorded quasi-simultaneously by line-by-line switching and recording with the illumination patterns described above (Figure 1E) and with dwell times as optimized for rsEGFP2 (Figure 2D). Such precise colocalization *in vivo* between the channels is not possible with frame-by-frame scanning because structures usually move slightly between frames, rendering colocalization studies impossible (Figure S4). Figures 3E–3G highlight some of the features that can be observed with this technique, such as the PSD95 nano-organization showing two distinct clusters (Figure 3E, asterisk) or horseshoe shape (Figure 3F, asterisk). Glutamatergic synapses are also formed on dendritic shafts (Figure 3G, asterisk) indicated by the overlap of the pre- and postsynaptic label on the dendrite without forming a spine. Line profiles show that the resolution in all three channels is below the diffraction limit (Figure 3H). Thus, our approach enables the super-resolution of the synaptic nano-organization and morphology for pre- and postsynaptic structures simultaneously. Such data can be used, for example, to quantify size correlations between pre- and postsynaptic elements. For instance, we performed here a small analysis of presynaptic vesicle cluster size and postsynaptic morphology. We identified spines carrying a PSD95 assembly that spatially overlaps with presynaptic synaptophysin. We manually encircled both at the largest extent and computed their area (Figure 3I). Likewise, we determined the area of the spine head cross-section (Figure 3I). Plotting the synaptophysin vesicle cluster area (Figure 3J) or PSD95 assembly area (Figure 3K) over spine head size revealed a linear correlation with a coefficient of determination of 0.41 in both cases. The vesicle cluster area, however, did not correlate with the size of the postsynapse (Figure 3L). This suggests a matching in size to some extent between pre- and postsynaptic elements.

Quasi-simultaneous dual-label STED microscopy by combining a positive and negative switching RSFP

Some time ago, we published an approach of dual-label STED microscopy in which we combined the positively switching RSFP Padron and the negatively switching RSFP Dronpa-M159T and recorded them in a single-color STED microscope (Willig et al., 2011). However, these images were recorded one after the other, i.e., frame by frame. We now applied our parallelized switching approach to neurons expressing myr-Dronpa-M159T to label the membrane and Lifeact-Padron for F-actin labeling. Images were recorded line by line with switching steps between image recordings (Figure 4A). While the membrane labeling shows the outline of a dendritic stretch (Figure 4B), actin forms thin fibers within the dendrite and its protrusions (Figures 4C and 4D). Thus, our parallelized switching approach enables the quasi-simultaneous imaging of a positive and negative switching RSFP. The imaging speed is mainly limited by the relatively slow switching Padron.

Time-lapse STED microscopy of multi-labels using RSFPs

By using RSFPs, on- and off-switching can be repeated several times so that several images of the same position can be recorded. This applies to both the three-label *in vivo* and the

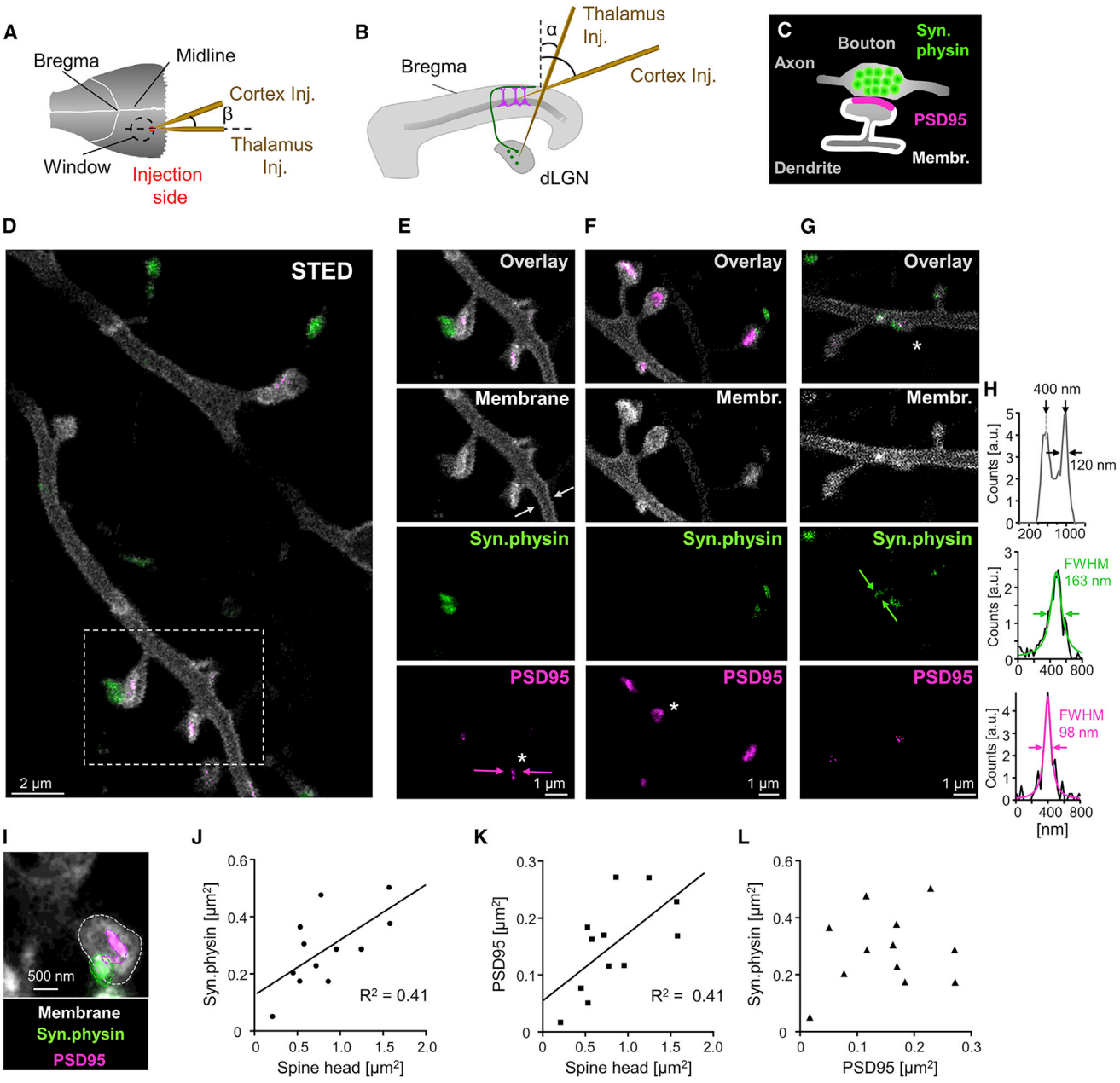

Figure 3. Triple-label *in vivo* STED microscopy of pre- and post-synapse in cerebral cortex of an anesthetized mouse

(A) Sides of viral injection and cranial window over the visual cortex of the left hemisphere.

(B) rAAVs injected into the dLGN encode for a synaptic vesicle marker (green) in thalamocortical neurons sending projections among others to layer 1 of the visual cortex. Injection at the same position but larger angle α transduces mainly layer 5 pyramidal neurons (magenta).

(C) Labeling schema: pyramidal neurons express the membrane marker myr-rsEGFP2-LDLR(Ct) (white) and postsynaptic marker PSD95-FingR-Citrine (magenta); presynaptic boutons of axonal projections accumulate synaptic vesicles, which are marked by synaptophysin-EGFP (green).

(D–G) *In vivo* STED images of synaptophysin (green, EGFP) in the presynaptic bouton and the postsynaptic dendritic membrane (white, rsEGFP2) and attached postsynaptic PSD95 (magenta, Citrine). Asterisks (*) mark a clustered nano-organization (E) or a horseshoe (F) distribution of PSD95 and a shaft synapse (G). (E) Marked area in (D).

(H) Line profiles and Lorentzian fit (straight line) of positions indicated by arrows in (E) and (G).

(I–L) Size correlation between overlapping pre- and postsynaptic elements. (I) Size measurement by encircling the largest extent of the spine head (white dashed line), PSD95 assembly (magenta dashed line), and synaptophysin vesicle cluster (green dashed line). (J–K) Synaptophysin vesicle cluster (J) and PSD95 (K) size correlate with spine head size (J, *p = 0.024; K, *p = 0.026, two-tailed Pearson correlation). R^2 is the coefficient of determination. Straight line depicts linear regression. (L) No significant correlation is observed between synaptophysin vesicle cluster and PSD95 size. (J–L) Twelve overlapping pre- and postsynaptic structures in three mice were analyzed. Images are maximum intensity projections (MIPs).

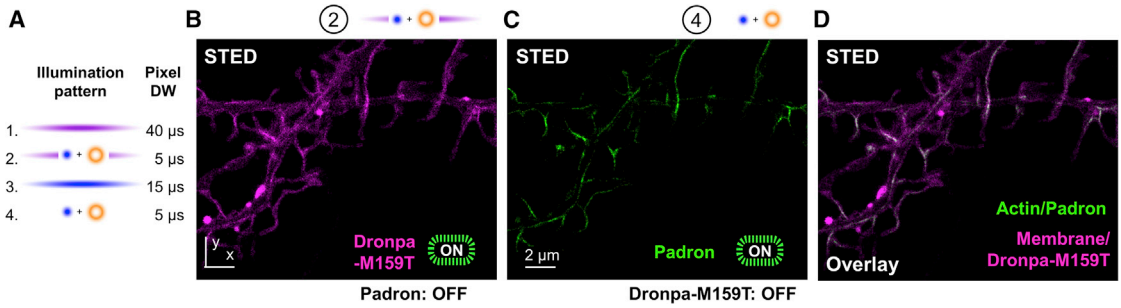

Figure 4. Quasi-simultaneous imaging of Padron- and Dronpa-M159T-labeled structures in living neuronal cultures

(A) Alternated line switching schema. The x axis was scanned four times with the indicated illumination pattern and pixel dwell time (DW).

(B and C) A dendrite expressing the membrane label myr-LDLR(Ct) fused to Dronpa-M159T and the F-actin label Lifeact-Padron was imaged with STED microscopy. Dronpa-M159T was detected in the second step (B) and Padron in the fourth step (C) with low cross-talk.

(D) Overlay of (B) and (C). Images are smoothed and displayed without unmixing of cross-talk.

dual-label strategy. Figure 5A shows a time-lapse recording of three image stacks recorded in the visual cortex of an anesthetized mouse labeled as explained in Figure 3. In the same image we observed a presynaptic bouton (green, synaptophysin) of a thalamocortical axonal projection and a branch of a layer 5 apical dendrite whose membrane was labeled (white, myr) and expressing a postsynaptic marker of glutamatergic synapses (magenta, PSD95). All three time points were recorded with STED microscopy showing the synaptic nano-organization and spine morphology at super-resolution.

Similarly, we recorded time-lapse STED images of Padron and Dronpa-M159T in living cells (Figure 5B). We labeled the membrane with Dronpa-M159T (magenta) and F-actin with Padron (green) in cultured hippocampal neurons as described above (Figure 4). Three STED microscopy images were recorded within ~5 min that show thin actin fibers in the dendrite and actin hotspots in the spine heads. The membrane label outlines the dendrite and attached spines. As expected at this time scale, we do not observe a significant change of morphology either *in vivo* (Figure 5A) or *in vitro* (Figure 5B).

Taken together, RSFPs can be utilized for time-lapse live-cell and *in vivo* STED microscopy. They extend multi-label STED microscopy on the temporal axis by utilizing reversible switching. Parallelized switching enables quasi-simultaneously recording line by line.

DISCUSSION

We present here an approach for multi-label STED microscopy based solely on genetically encoded fluorescent proteins. To our knowledge, this is the first super-resolution imaging of three labels in the living mouse cortex. Instead of extending the spectral range and adding another fluorescence color, we apply temporal sequential imaging. Key to the proposed method's power for *in vivo* imaging is our parallelized switching approach that enables fast quasi-simultaneous imaging. There are no specific requirements on the temporal stability or beam profile of the switching lasers, and thus cheap lasers or even laser pointers can be used as a light source. This approach is therefore technically relatively simple and cost-efficient. By recording the channels sequentially, a one-color STED microscope is basically sufficient for dual-label imaging and a two-color STED microscope for triple-label imaging. Because we employ only a single STED beam, all images are inherently aligned without suffering chromatic aberrations.

Multi-label super-resolution imaging in the mouse cerebral cortex offers a wide range of potential applications, such as, for example, the determination of the correlation of spine morphology with presynaptic vesicle cluster sizes and PSD95 nanostructure. Moreover, it enables the investigation of temporal changes of pre- and postsynaptic nano-organizations at baseline, with dedicated stimulation protocols and/or in mouse models of brain diseases. A large range of available mouse driver lines or genetic tools enable a pathway- or activity-specific morphological analysis of the synaptic nanostructure. Furthermore, EGFP could be substituted, for example, with the genetically encoded calcium indicator GCaMP6 (Chen et al., 2013) for imaging of neuronal activity, with or without stimulated depletion. Another potential application is to study the interaction of fine processes of astrocytes with synapses, which are often described as the "tripartite synapse" and whose role in synaptic transmission remains unknown (Bernardinelli et al., 2014).

In principle, it should be possible to use RSFPs also for two-photon excitation STED microscopy (Bethge et al., 2013; Coto Hernández et al., 2016). However, it needs to be tested whether the two-photon beam affects the switching contrast by activating or deactivating the RSFP.

Besides their spectral properties, the RSFPs were selected for the following reasons. First, we had already used Dronpa-M159T before (Willig et al., 2011), and it is a fast-switching RSFP. rsEGFP2 was specifically developed and optimized for mammalian expression, is truly monomeric, and is as well fast switching (Grotjohann et al., 2012). Indeed, the expression of rsEGFP2 was better than Dronpa-M159T in mice, and therefore we employed rsEGFP2 for *in vivo* experiments. The STED resolution of rsEGP2 is very similar to that of EGFP, probably reflecting that rsEGFP2 is a derivative of EGFP (Grotjohann et al., 2011, 2012).

In our dual-label approach, we switch between the on states of Padron and Dronpa-M159T. Currently, the imaging speed of this configuration is mainly limited by the relatively slow switching

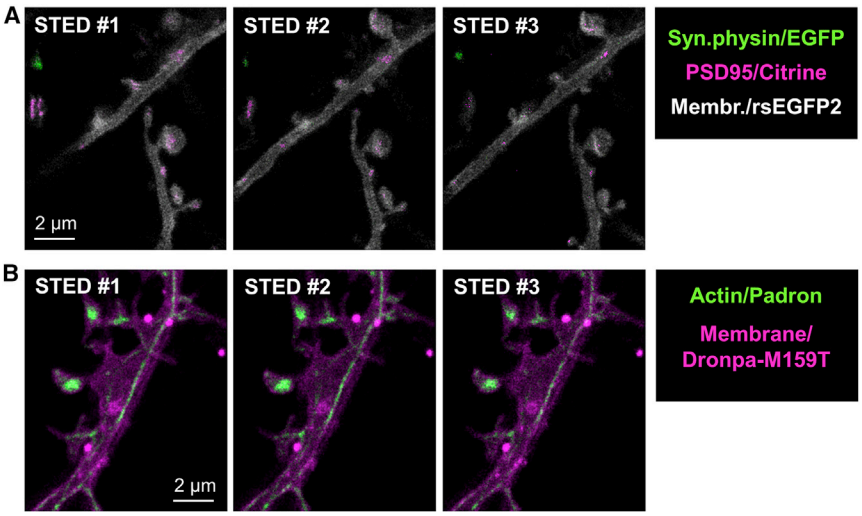

Figure 5. Time-lapse STED microscopy of multi-labels

(A) Triple-label *in vivo* STED microscopy of EGFP (green, synaptophysin), Citrine (magenta, PSD95), and rsEGFP2 (white, membrane) at three time points recorded directly one after the other in layer 1 of the mouse visual cortex. Images are maximum intensity Imaging settings are as in Figure 3.

(B) Dual-label life-cell STED microscopy of the RSFPs Padron (green, Lifeact) and Dronpa-M159T (magenta, myr) at three time points directly one after the other. Living cultured neuron. Imaging settings are as in Figure 4.

speed of Padron. Due to their use in RESOLFT microscopy, much effort has been invested into the development of negative switching RSFPs like rsEGFP2, while positive switching RSFPs have so far not been systematically improved. Thus, there is presumably a large potential to increase the switching speed of Padron in the future.

The dual-label approach utilizing Padron and Dronpa-M159T exhibits only low cross-talk and thus does not require computational processing. The combination of conventional fluorescent proteins and RSFPs for triple labeling nevertheless requires image processing. Although EGFP and Citrine are imaged virtually free of cross-talk, the rsEGFP2 image is superimposed with the EGFP image. The EGFP image, however, can be easily subtracted to gain the pure rsEGFP2 image. For colocalization studies, however, it would be advisable to use EGFP and Citrine for the proteins with the strongest overlap.

Lastly, it should be noted that imaging parameters such as excitation power and pixel dwell time do influence the switching capability. For example, a higher laser power would increase switching speed but at the same time induce bleaching. All imaging parameters presented here were therefore optimized first for parallelized switching with the line illumination. Thereafter, all switching schemas were imaged with the same excitation power and dwell time for comparison.

Overall, RSFPs are an important addition to the family of STED suitable live-cell and *in vivo* markers. They can be read out sequentially in time by extending the labeling strategy on the temporal axis without enhancing the complexity of the STED microscope. The triple-label *in vivo* STED microscopy approach is applicable as well for longitudinal STED imaging and/or imaging of activity-driven changes.

STAR★METHODS

Detailed methods are provided in the online version of this paper and include the following:

SUPPLEMENTAL INFORMATION

Supplemental information can be found online at https://doi.org/10.1016/j.celrep.2021.109192.

ACKNOWLEDGMENTS

We thank Dr. Carola Gregor, Max Planck Institute for Biophysical Chemistry, Göttingen, for cloning of pAAV-hSyn-Lifeact-Padron; Dr. Birka Lalkens and Dr. Fred Wolf for critical reading; and Dr. Karl Deisseroth, Stanford University, Dr. Silvio Rizzoli, University Medical Center Göttingen, and Dr. Stefan Jakobs, Max Planck Institute for Biophysical Chemistry, Göttingen, for providing plasmids. This work was supported by the Deutsche Forschungsgemeinschaft (DFG, German Research Foundation) within the DFG Research Center and Cluster of Excellence (EXC 171, Area A1) "Nanoscale Microscopy and Molecular Physiology of the Brain"; the Göttingen Cluster for Multiscale Bioimaging EXC 2067/1-390729940 (K.I.W.); the Collaborative Research Center 889 "Cellular Mechanisms of Sensory Processing" (Project B7) (A.M., K.I.W.); the Göttingen Graduate Center for Neurosciences, Biophysics, and Molecular Biosciences (VCF); and the Open Access Publication Funds of Göttingen University.

AUTHOR CONTRIBUTIONS

Conceptualization, K.I.W.; STED microscope design and construction, K.I.W.; imaging, K.I.W.; transduction and craniotomy, H.S. and W.W.; cloning and

virus production, W.W. and A.M.; neuronal culture, V.C.-F.; writing, K.I.W.; supervision, K.I.W.

DECLARATION OF INTERESTS

K.I.W. and the Max Planck Society filed a patent application on the parallelized switching approach.

Received: January 21, 2021
Revised: April 8, 2021
Accepted: May 7, 2021
Published: June 1, 2021

REFERENCES

Beater, S., Holzmeister, P., Lalkens, B., and Tinnefeld, P. (2015). Simple and aberration-free 4color-STED—multiplexing by transient binding. Opt. Express *23*, 8630–8638.

Bernardinelli, Y., Randall, J., Janett, E., Nikonenko, I., König, S., Jones, E.V., Flores, C.E., Murai, K.K., Bochet, C.G., Holtmaat, A., and Muller, D. (2014). Activity-dependent structural plasticity of perisynaptic astrocytic domains promotes excitatory synapse stability. Curr. Biol. *24*, 1679–1688.

Berning, S., Willig, K.I., Steffens, H., Dibaj, P., and Hell, S.W. (2012). Nanoscopy in a living mouse brain. Science *335*, 551.

Bethge, P., Chéreau, R., Avignone, E., Marsicano, G., and Nägerl, U.V. (2013). Two-photon excitation STED microscopy in two colors in acute brain slices. Biophys. J. *104*, 778–785.

Blom, H., and Widengren, J. (2017). Stimulated Emission Depletion Microscopy. Chem. Rev. *117*, 7377–7427.

Bottanelli, F., Kromann, E.B., Allgeyer, E.S., Erdmann, R.S., Wood Baguley, S., Sirinakis, G., Schepartz, A., Baddeley, D., Toomre, D.K., Rothman, J.E., and Bewersdorf, J. (2016). Two-colour live-cell nanoscale imaging of intracellular targets. Nat. Commun. *7*, 10778.

Bückers, J., Wildanger, D., Vicidomini, G., Kastrup, L., and Hell, S.W. (2011). Simultaneous multi-lifetime multi-color STED imaging for colocalization analyses. Opt. Express *19*, 3130–3143.

Chen, T.-W., Wardill, T.J., Sun, Y., Pulver, S.R., Renninger, S.L., Baohan, A., Schreiter, E.R., Kerr, R.A., Orger, M.B., Jayaraman, V., et al. (2013). Ultrasensitive fluorescent proteins for imaging neuronal activity. Nature *499*, 295–300.

Chen, H., Tang, A.H., and Blanpied, T.A. (2018). Subsynaptic spatial organization as a regulator of synaptic strength and plasticity. Curr. Opin. Neurobiol. *51*, 147–153.

Coto Hernández, I., Castello, M., Lanzanò, L., d'Amora, M., Bianchini, P., Diaspro, A., and Vicidomini, G. (2016). Two-Photon Excitation STED Microscopy with Time-Gated Detection. Sci. Rep. *6*, 19419.

Cruz-Martín, A., El-Danaf, R.N., Osakada, F., Sriram, B., Dhande, O.S., Nguyen, P.L., Callaway, E.M., Ghosh, A., and Huberman, A.D. (2014). A dedicated circuit links direction-selective retinal ganglion cells to the primary visual cortex. Nature *507*, 358–361.

D'Este, E., Kamin, D., Balzarotti, F., and Hell, S.W. (2017). Ultrastructural anatomy of nodes of Ranvier in the peripheral nervous system as revealed by STED microscopy. Proc. Natl. Acad. Sci. USA *114*, E191–E199.

Eggeling, C., Willig, K.I., Sahl, S.J., and Hell, S.W. (2015). Lens-based fluorescence nanoscopy. Q. Rev. Biophys. *48*, 178–243.

Göttfert, F., Wurm, C.A., Mueller, V., Berning, S., Cordes, V.C., Honigmann, A., and Hell, S.W. (2013). Coaligned dual-channel STED nanoscopy and molecular diffusion analysis at 20 nm resolution. Biophys. J. *105*, L01–L03.

Gross, G.G., Junge, J.A., Mora, R.J., Kwon, H.-B.B., Olson, C.A., Takahashi, T.T., Liman, E.R., Ellis-Davies, G.C.R.R., McGee, A.W., Sabatini, B.L., et al. (2013). Recombinant probes for visualizing endogenous synaptic proteins in living neurons. Neuron *78*, 971–985.

Grotjohann, T., Testa, I., Leutenegger, M., Bock, H., Urban, N.T., Lavoie-Cardinal, F., Willig, K.I., Eggeling, C., Jakobs, S., and Hell, S.W. (2011). Diffraction-unlimited all-optical imaging and writing with a photochromic GFP. Nature *478*, 204–208.

Grotjohann, T., Testa, I., Reuss, M., Brakemann, T., Eggeling, C., Hell, S.W., and Jakobs, S. (2012). rsEGFP2 enables fast RESOLFT nanoscopy of living cells. eLife *1*, e00248.

Herring, B.E., and Nicoll, R.A. (2016). Long-Term Potentiation: From CaMKII to AMPA Receptor Trafficking. Annu. Rev. Physiol. *78*, 351–365.

Jensen, N.A., Jansen, I., Kamper, M., and Jakobs, S. (2020). Reversibly switchable fluorescent proteins for RESOLFT nanoscopy. In Nanoscale Photonic Imaging, T. Salditt, A. Egner, and D. Luke, eds. (Springer International Publishing), pp. 241–261.

Kameda, H., Furuta, T., Matsuda, W., Ohira, K., Nakamura, K., Hioki, H., and Kaneko, T. (2008). Targeting green fluorescent protein to dendritic membrane in central neurons. Neurosci. Res. *61*, 79–91.

Masch, J.-M., Steffens, H., Fischer, J., Engelhardt, J., Hubrich, J., Keller-Findeisen, J., D'Este, E., Urban, N.T., Grant, S.G.N., Sahl, S.J., et al. (2018). Robust nanoscopy of a synaptic protein in living mice by organic-fluorophore labeling. Proc. Natl. Acad. Sci. USA *115*, E8047–E8056.

Schindelin, J., Arganda-Carreras, I., Frise, E., Kaynig, V., Longair, M., Pietzsch, T., Preibisch, S., Rueden, C., Saalfeld, S., Schmid, B., et al. (2012). Fiji: an open-source platform for biological-image analysis. Nat. Methods *9*, 676–682.

Schneider, A.F.L., and Hackenberger, C.P.R. (2017). Fluorescent labelling in living cells. Curr. Opin. Biotechnol. *48*, 61–68.

Sidenstein, S.C., D'Este, E., Böhm, M.J., Danzl, J.G., Belov, V.N., and Hell, S.W. (2016). Multicolour multilevel STED nanoscopy of actin/spectrin organization at synapses. Sci. Rep. *6*, 26725.

Steffens, H., Wegner, W., and Willig, K.I. (2020). In vivo STED microscopy: A roadmap to nanoscale imaging in the living mouse. Methods *174*, 42–48.

Tønnesen, J., Nadrigny, F., Willig, K.I., Wedlich-Söldner, R., and Nägerl, U.V. (2011). Two-color STED microscopy of living synapses using a single laser-beam pair. Biophys. J. *101*, 2545–2552.

Wegner, W., Ilgen, P., Gregor, C., van Dort, J., Mott, A.C., Steffens, H., and Willig, K.I. (2017). In vivo mouse and live cell STED microscopy of neuronal actin plasticity using far-red emitting fluorescent proteins. Sci. Rep. *7*, 11781.

Willig, K.I., Stiel, A.C., Brakemann, T., Jakobs, S., and Hell, S.W. (2011). Dual-label STED nanoscopy of living cells using photochromism. Nano Lett. *11*, 3970–3973.

Willig, K.I., Steffens, H., Gregor, C., Herholt, A., Rossner, M.J., and Hell, S.W. (2014). Nanoscopy of filamentous actin in cortical dendrites of a living mouse. Biophys. J. *106*, L01–L03.

Winter, F.R., Loidolt, M., Westphal, V., Butkevich, A.N., Gregor, C., Sahl, S.J., and Hell, S.W. (2017). Multicolour nanoscopy of fixed and living cells with a single STED beam and hyperspectral detection. Sci. Rep. *7*, 46492.

STAR★METHODS

KEY RESOURCES TABLE

REAGENT or RESOURCE	SOURCE	IDENTIFIER
Chemicals, peptides, and recombinant proteins		
Fentanyl® (Fentanyl citrate)	Janssen	CAS 990-73-8
Midazolam-ratiopharm® (hydrochloride)	Ratiopharm	CAS 59467-96-8
Dormilan® (Medetomidine hydrochloride)	Alfavet	CAS 86347-15-1
Histoacryl® (n-butyl-2-cyanoacrylate)	B. Braun Melsungen AG	CAS 006606-65-1
Super-Bond C&B	Sun Medical Co. LTD	N/A
Experimental models: Organisms/strains		
Mouse: C57BL/6J	JAX	RRID:IMSR_JAX:000664
Oligonucleotides		
Primers for pAAV-hSyn-XXX see Table S1	This paper	N/A
Recombinant DNA		
pAAV-hSyn-Cre	Wegner et al., 2017	N/A
pAAV-hSyn-DIO-myr-DronpaM159T-LDLR	This study	N/A
pAAV-hSyn-DIO-myr-rsEGFP2-LDLR	This study	N/A
pAAV-hSyn-Lifeact-rsEGFP2	This study	N/A
pAAV-hSyn-Lifeact-Padron	This study	N/A
pAAV-hSyn-Synaptophysin-EGFP	This study	N/A
pAAV-ZFN-hSyn-DIO-PSD95-FingR-Citrine-CCR5TC	This study	N/A
Software and algorithms		
Fiji/ImageJ	Schindelin et al., 2012	RRID:SCR_002285
GraphPad Prism	GraphPad	RRID:SCR_002798
Imspector Software	Abberior Instruments	RRID:SCR_015249

RESOURCE AVAILABILITY

Lead contact

Further information and requests for resources and reagents should be directed to and will be fulfilled by the Lead Contact Katrin I. Willig (Email: kwillig@em.mpg.de)

Materials availability

Requests for plasmids should be directed to and will be fulfilled by the Lead Contact Katrin I. Willig

Data and code availability

Requests for image datasets should be directed to the Lead Contact KIW (kwillig@em.mpg.de) and will be made available upon reasonable request. No code was generated.

EXPERIMENTAL MODEL AND SUBJECT DETAILS

Animals

All experiments were performed according to the guidelines of the national law regarding animal protection procedures and were approved by the responsible authorities, the Niedersächsisches Landesamt für Verbraucherschutz (LAVES, identification number 33.9-42502-04-14/1463 and −18/2819). All efforts were made to minimize animal suffering and the number of animals used. C57BL/6J mice were reared at the animal facility of the Max Planck Institute of Experimental Medicine in Göttingen and housed in groups with a 12 h light/dark cycle, with food and water *ad libitum*. Four female mice were transduced at the age of 10–17 weeks and imaged 3–6 weeks after transduction.

CellPress
OPEN ACCESS

METHOD DETAILS

Triple-label STED microscopy

For triple-label STED microscopy we added lasers and scanning modalities to a custom-designed STED microscope (Willig et al., 2014) as follows (Figure 1A). Excitation of EGFP and rsEGFP2 was provided by a pulsed laser diode (Exc1) emitting blue light at 483 nm (PiLas, Advanced Laser Diode Systems, Berlin, Germany). Pulsed excitation of Citrine was accomplished by filtering white light of a supercontinuum device (FemtoWHITE800, NKT photonics, Birkerød, Denmark) for 520 nm green light (Exc2) with a band-pass filter (BrightLine HC 520/5, Semrock, IDEX Health & Science, Rochester, NY). The supercontinuum device was pumped by a Ti:Sapphire laser (MaiTai; Spectra-Physics, Santa Clara, CA) which was also pumping an optical parametric oscillator (OPO, APE, Berlin, Germany) to generate the pulsed STED light at 595 nm. Exc1, Exc2 and the STED beam were spatially superimposed by dichroic mirrors; after passing relay optics and a Yanus scan head (Till Photonics-FEI, Gräfelfing, Germany) the three beams were focused by a 1.3 numerical aperture objective lens (PL APO, 63x, glycerol; Leica, Wetzlar, Germany). Temporal overlap of the pulses of Exc1 and the STED laser in the focal spot was achieved electronically. Exc2 was synchronized with the STED pulses by an optical delay line. The STED beam was passing a vortex phase plate (VPP; RPC Photonics, Rochester, NY) to create a doughnut shaped focal intensity pattern featuring zero intensity in the center. For switching of the RSFPs we incorporated a continuous wave laser emitting at 488 nm (Switch1; Cobolt 06-MLD, HÜBNER Photonics, Kassel, Germany) with a dichroic mirror (DM1, zt473rdcxt, Chroma Technology Corporation, Bellow Falls, VT) and a 405 nm continuous wave laser (Switch2; Cobolt 06-MLD) via a polarizing beam splitter cube (PBS, Thorlabs, 420-680 nm, Thorlabs Inc., Newton, NJ). To create a line pattern in the focal plane we placed a cylindrical lens of 150 mm focal length (CL1, plano-convex cylindrical lens, Thorlabs) in the 488 mm beam path and of 250 mm focal length (CL2, Thorlabs) in the 405 nm beam path focusing into the conjugated plane of the back aperture of the objective. All laser beams were spatially cleaned up by passing a polarization preserving, single-mode fiber (SMF). The back-projected fluorescence light was split at 515 nm with a dichroic mirror (DM3, ZT502rdc-UF3; Chroma Technology) into two beams. The shorter wavelength was reflected and spectrally filtered for 498–510 nm by a band-pass filter (Det1; BrightLine HC 504/12; Semrock) and detected by a single photon counting module (SPCM-AQRH, Excelitas, Waltham, MA) after passing a multi-mode fiber (MMF) which acts as a confocal pinhole. The longer wavelength fluorescence light was filtered for 532–555 nm with a bandpass filter (Det2; H544/23, AHF analysentechnik, Tübingen, Germany) and detected by a SPCM, respectively. Data acquisition was performed with an Abberior Patchpanel and the software Imspector (Abberior Instruments, Göttingen, Germany).

Plasmid and virus production

Plasmid generation was performed by conventional PCR-based cloning including amplification of the desired DNA sequence, followed by restriction endonuclease digestion and subsequent ligation. All primers and restriction endonuclease used are listed in Table S1. To generate the construct pAAV-hSyn-DIO-myr-DronpaM159T-LDLR(Ct)-WPRE, several cloning steps were carried out. First, we generated pAAV-hSyn-DIO-EYFP by replacing the human elongation factor-1 alpha (Ef1a) promoter with the human Synapsin promoter (hSyn) of the pAAV-Ef1a-DIO-EYFP plasmid, kindly provided by Dr. Karl Deisseroth, Stanford University, CA; DIO refers to double-floxed inverted open reading frame. Next, three different PCR fragments were amplified or hybridized, digested, and ligated into the pAAV-hSyn-DIO-EYFP backbone: First, the myristoylation site (myr) ATGGGCTGTGTGCAATGTAAGGATAAAGAAGCAACAAAACTGACG was attached to the DronpaM159T sequence (denoted by DronpaM159T$^{v2.0}$ in Willig et al., 2011) by using a forward primer containing the myr site. Second, the C-terminal (Ct) cytoplasmic domains of low density lipoprotein receptor (LDLR; GenBank: AF425607, amino acid residues 813–862) (Kameda et al., 2008), were divided into two segments (segment 1 and 2). For each segment a pair of 5′-phsophorylated primers were designed and hybridized (Table S1). In the final step, all three DNA fragments, my-DronpaM159T, LDLR segment 1 and 2 were ligated into the pAAV-hSyn-DIO-EYFP vector, to finally generate the pAAV-hSyn-DIO-my-DronpaM159T-LDLR(Ct) construct. For the preparation of the plasmid pAAV-hSyn-DIO-myr-rsEGFP2-LDLR(Ct) the fluorescent protein DronpaM159T was exchanged against rsEGFP2 (provided by Dr. Stefan Jakobs, MPI for Biophysical Chemistry, Göttingen, Germany) (Grotjohann et al., 2012).

The construct pAAV-hSyn-DIO-Lifeact-rsEGFP2 was created in two consecutive steps. First, the fluorescent protein mNeptune2 of the construct pAAV-hSyn-Lifeact-mNeptune2 (Wegner et al., 2017) was exchanged for rsEGFP2 to generate the intermediate construct pAAV-hSyn-Lifeact-rsEGFP2. Subsequently, the Lifeact-rsEGFP2 sequence was introduced into the backbone of pAAV-hSyn-DIO-EYFP, deleting EYFP.

For pAAV-hSyn-Lifeact-Padron, tagRFP657 was replaced by Padron (denoted by Padron$^{v2.0}$ in Willig et al., 2011) in the construct pAAV-hSyn-Lifeact-tagRFP657 (Wegner et al., 2017).

The presynaptic marker construct pAAV-hSyn-Synaptophysin-EGFP, which is not double inverted, was created by cloning the sequence of Synaptophysin-EGFP from the construct pEGFP_N1_Synaptophysin_EGFP (provided by Dr. Silvio Rizzoli, University Medical Center Göttingen, Germany) into the pAAV-hSyn-DIO-EYFP vector, including deletion of lox-P sites.

The plasmid pAAV-ZFN-hSyn-DIO-PSD95-FingR-Citrine-CCR5TC encoding the transcriptionally regulated postsynaptic marker of PSD95 was sequentially cloned by creating the following plasmids: 1) pAAV-ZFN-hSyn-DIO-EYFP: Insertion of the zinc finger binding motif (ZFN) (Gross et al., 2013) upstream of the hSyn promoter into pAAV-hSyn-DIO-EYFP by hybridization of two 5′-phosphorylated primers. 2) pAAV-ZFN-hSyn-DIO-PSD95-FingR-Citrine-CCR5TC: PCR based insertion of the antibody like PSD95-FingR (FingR: Fibronectin intrabodies generated with mRNA display) (Gross et al., 2013), the transcriptionally regulatory elements

CCR5ZFL-KRAB(A) (CCR5ZFL: left zinc finger from an engineered zinc-finger nuclease against the gene CCR5; KRAB(A): transcriptional repressor domain from rat Kid-1 (Gross et al., 2013), and the fluorescent protein Citrine. PSD95-FingR and CCR5ZFL-KRAB(A) were amplified from plasmid pCAG_PSD95.FingR-eGFP-CCR5TC (gift from Dr. Don Arnold (Addgene plasmid # 46295)).

The cre recombinase expression plasmid pAAV-hSyn-Cre is described in Wegner et al. (2017).

Recombinant adeno-associated viral particles (rAAV) with mixed serotype 1 and 2 were produced as described in Wegner et al. (2017).

Cultured neurons and live cell imaging

Primary cultures of rat hippocampal neurons were prepared from P0-P1 Wistar rats (RjHan:WI; The Jackson Laboratory, Bar Harbor, ME) of both sex according to D'Este et al. (2017). Neurons were cultured at 37°C in a humidified atmosphere with 5% CO_2 and transduced between 7 and 8 days *in vitro* (DIV) with the respective rAAVs. After an incubation time of 7 days, live cell STED imaging was performed at room temperature in neuronal culture medium.

Mouse transduction

Mice were anaesthetized by i.p. injection of 0.05 mg/kg Fentanyl (CAS 990-73-8), 5 mg/kg Midazolam (CAS 59467-96-8), and 0.5 mg/kg Medetomidine (CAS 86347-15-1). A gas mixture with a high O_2 (47.5 vol %) and CO_2 (2.5 vol %) content was administered over a cone in front of the mouse's nose to significantly increase the oxygenation. Pulse rate and O_2 saturation were measured with a pulse oximeter (MouseOx STARR®, STARR Life Science Corp., Oakmont, PA) on the mouse thigh to monitor the depth of the anesthesia. The mouse was head fixed in a stereotaxic frame (Narishige, Tokyo, Japan) and placed on a heating pad throughout the procedure to maintain a constant body temperature, which was monitored with a rectal temperature probe. After disinfection the skin was cut by a ~0.5 cm long incision and a drop of local anesthetic (0.2 mg Mepivacaine) was applied. Then, a 0.5 mm hole was drilled (RUDOLF FLUME Technik GmbH, Essen, Germany) 3.4 mm caudal of Bregma and 2.15 mm lateral of the midline. Thalamus injection was performed at $\alpha = 30°$ to the vertical and parallel to the midline (Figures 3A and 3B); a glass micropipette attached to a microinjector (Picospritzer® III, Parker Hannifin Corp, Cleveland, Ohio) was inserted 2.75 mm and ~150 nL of rAAV encoding for synaptophysin-EGFP were injected over ~3 min. After letting it settle for a few minutes the pipette was removed and cortex injection was performed at the same position. Therefore, a micropipette containing a mixture of rAAV encoding for myr-rsEGFP2, PSF95-FingR-Citrine and cre was inserted 0.75 mm at $\alpha = 70°$ to the vertical and $\beta = 20°$away from the midline and ~300 nL of solution were injected. The incision was closed with a suture and anesthesia was antagonized by i.p. administration of 0.1 mg/kg Buprenorphine (CAS 53152-21-9) and 2.5 mg/kg Atipamezole (CAS 104075-48-1).

In vivo STED imaging

Three to six weeks after viral transduction, a craniotomy was performed as previously described (Steffens et al., 2020). In brief, the mouse was anaesthetized and vital functions were monitored as described above for transduction. The head was mounted in a stereotaxic frame and the scalp was removed. A head bar was glued to the right hemisphere to leave enough space for the cranial window above the visual cortex, rostral to the former injection site. After drilling a circular groove (~2-3 mm) into the skull, the bony plate was carefully removed as atraumatic as possible. The remaining dura and arachnoid mater were carefully removed with a fine forceps and a small tube was positioned at the edge of the craniotomy to drain excess cerebrospinal fluid if necessary. Then, the craniotomy was sealed with a 6 mm diameter cover glass glued to the skull. The mouse was mounted on a tiltable plate and aligned perpendicular to the optical axis of the microscope before being placed under the microscope (Steffens et al., 2020). STED microscopy was performed in layer 1 of the visual cortex at a depth of 5–20 μm below the pia. The correction collar of the glycerol immersion objective was adjusted at each depth to compensate for spherical aberrations in the tissue in order to optimize the STED resolution. *In vivo* images were recorded with a pixel size of 30 × 30 nm in x and y and z stacks in steps of 600 nm. Blue and green excitation was 4.5 μW, respectively. The average STED power was 28 mW (Figures 3D–3F and S4), 19 mW (Figures 3G, 5A, and 5B), 37 mW (Figure 4). Switching with a line pattern was performed with a power of 10 μW for 405 nm and 25 μW for 488 nm. All values correspond to the power at the back aperture of the objective. The STED resolution was determined in Figure S2 for a STED power of 37 mW and 42 mW and scales with the inverse square root of the STED laser power (Eggeling et al., 2015).

QUANTIFICATION AND STATISTICAL ANALYSIS

Image processing and size analysis

All images were smoothed with a low pass filter over 2 pixels in the software Imspector (Abberior Instruments). The selective excitation of EGFP with 483 nm and detection in detection channel 1 (Det1) and excitation of Citrine with 520 nm and detection with channel 2 (Det2) were virtually free of cross-talk and no further computational processing such as channel unmixing was required. Excitation of rsEGFP2 with 483 nm excited also EGFP and to a small, but negligible fraction Citrine. The main portion of rsEGFP2 fluorescence was detected in detection channel 1 (Det1) and a small portion in channel 2 (Det2). To increase the signal-to-noise ratio we added up both detection channels (Det1+Det2) for rsEGFP2. Due to the summation of both detection channels the signal of the cross-talk of EGFP into the rsEGFP2 detection is different than the sole EGFP signal detected only in channel 1. Thus, we measured the signal intensity of EGFP structures which were not spatially overlapping with the rsEGFP2 in the EGFP

and rsEGFP2 channel. Then, we scaled the EGFP image to reach the intensity of EGFP in the rsEGFP2 channel and thereafter subtracted the scaled EGFP image from the rsEGFP2 image.

Line profiles show an average of three lines.

Spines with overlapping synaptophysin, PSD95 and spine head labeling were identified and analyzed manually using Fiji (Schindelin et al., 2012). The images were smoothed (average over 3 pixels) and the postsynaptic spine head and PSD95 assembly and presynaptic vesicle cluster labeled via synaptophysin were encircled in the respective channel with the freehand selection tool to compute the area. Each structure was analyzed in its focal (x-y-) plane. Fitting and statistical analysis was performed in GraphPad Prism. Statistical significance was defined by $*p < 0.05$ and is specified in the figure legend.